Journal of Alloys and Compounds 517 (2012) 149–156

Contents lists available at SciVerse ScienceDirect

Journal of Alloys and Compounds

journal homepage: www.elsevier.com/locate/jallcom

Synthesis and luminescence properties of Y_2O_3:Eu with flower-like microstructure

Xuemei Zhang[a,b], Jiao Wang[a,b], Kai Guo[a,b], Haohong Chen[a], Xinxin Yang[a], Jingtai Zhao[a,*]

[a] Key Laboratory of Transparent Opto-functional Inorganic Materials of Chinese Academy of Sciences, Shanghai Institute of Ceramics, 1295 Ding Xi Road, Shanghai 200050, PR China
[b] Graduate School of Chinese Academy of Sciences, Beijing 100039, PR China

ARTICLE INFO

Article history:
Received 18 July 2011
Received in revised form
14 December 2011
Accepted 15 December 2011
Available online 24 December 2011

Keywords:
Microstructure
Y_2O_3:Eu
Hydrothermal
Luminescence

ABSTRACT

Europium-doped yttrium hydroxide ($Y(OH)_3$:Eu) with flower-like microstructure has been successfully prepared *via* a facile hydrothermal process, using potassium sodium tartrate ($C_4H_4O_6KNa$) as a structure-directing reagent. Europium-doped yttrium oxide (Y_2O_3:Eu) with similar morphology is prepared by calcining the as-prepared $Y(OH)_3$:Eu at 700 °C for 4 h. Influencing factors such as the concentration of potassium sodium tartrate, the amount of sodium hydroxide, and the temperature used for hydrothermal synthesis are systematically investigated. Possible formation mechanism for the flower-like microstructure is proposed on the basis of time-dependent experiment. Y_2O_3:Eu samples show a strong red emission corresponding to the $^5D_0$-$^7F_2$ transition of Eu^{3+} ions under excitation. Emission intensity varies between samples with different morphologies. The optimum Eu^{3+} doping concentration is also explored. This work sheds some light on the design and preparation of novel microstructures.

1. Introduction

Properties of inorganic functional materials are not only determined by their chemical composition but also tuned by their crystal structure, size, shape, and crystalline [1–5]. For a certain material with definite crystal structure, morphology may influence its property greatly [6–10]. Consequently, design and synthesis of inorganic functional materials with tunable sizes and well-defined morphologies remain a hot topic of scientific research.

Y_2O_3, as an important engineering materials, has potential applications in various fields, such as white LED phosphors [11], upconversion materials [12,13] and transparent ceramics [14]. In particular, Y_2O_3:Eu is a dominate red emitting materials in commercial application on fluorescent lighting and display, due to its good luminescent characteristics, acceptable atmospheric stability, reduced degradation under applied voltages, and lack of hazardous constituents as opposed to sulfide phosphors [15]. As a result, study on the luminescence properties of nano-/microcrystalline Y_2O_3:Eu has attracted extensive interest over the past decades. Y_2O_3:Eu phosphors with various morphologies have been prepared. 0-demensional Y_2O_3:Eu nanoparticles were successfully prepared through combustion [16], co-precipitation [17] and microemulsion-microwave method [18]. One-dimensional Y_2O_3:Eu nanostructures were also synthesized through various ways, such as nanotubes fabricated from nanolamellar precursors by a hydrothermal method [19], nanofiber prepared *via* electrospinning [20], nanobelts [21] and nanorods [22] synthesized through a hydrothermal method. Two-dimensional Y_2O_3:Eu nanostructures such as nanosheets [23] were also obtained.

However, it is still a great challenge to control the morphologies of three-dimensional microstructures, which are helpful to achieve a better understanding of crystal growth behavior, enrich the synthesis science, and find novel properties of existing materials. In the past few years, synthesis of Y_2O_3:Eu microstructure has received increasing attention. Up to now, Y_2O_3:Eu hollow spheres [24], microprisms [25], and microcubes [26] have been reported. However, precise and rational design and preparation of novel Y_2O_3:Eu microstructures remain a difficult task. In particular, the formation mechanisms of these novel microstructures need further investigation.

In the present work, $Y(OH)_3$:Eu with flower-like microstructure has been successfully synthesized in a tartrate-assisted hydrothermal condition. Y_2O_3:Eu with similar morphology is obtained after a following heat treatment. The concentration of reactants and reaction temperature are found to play crucial roles in controlling the particle size and shape of $Y(OH)_3$:Eu. A possible formation mechanism of the novel flower-like microstructure is proposed. And luminescence property study reveals that both particle morphology and Eu^{3+} ions doping concentration can influence the luminescence property of Y_2O_3:Eu.

* Corresponding author. Tel.: +86 21 52412073; fax: +86 21 52413122.
E-mail address: jtzhao@mail.sic.ac.cn (J. Zhao).

0925-8388/$ – see front matter © 2011 Elsevier B.V. All rights reserved.
doi:10.1016/j.jallcom.2011.12.068

2. Experimental

2.1. Synthesis procedures

All the reagents were of analytical purity and used without further purification. $Y(NO_3)_3$ and $Eu(NO_3)_3$ aqueous solution were obtained by dissolving Y_2O_3 and Eu_2O_3 in dilute HNO_3. In a typical procedure, 1 mmol $Y(NO_3)_3$ and 0.05 mmol $Eu(NO_3)_3$ were both added into 20 ml deionized water. Then 1 mmol potassium sodium tartrate tetrahydrate (PSTT) ($C_4H_4O_6KNa{\cdot}4H_2O$) was dissolved in the above solution under vigorous stir for 30 min. Then aqueous solution which contained 0.02 mol NaOH was added and the total volume was about 40 ml. After stirring for 30 min, the mixture was transferred to a 50 ml Teflon-lined stainless steel autoclave and kept at 210 °C for 12 h. When the autoclave cooled to room temperature naturally, the precursor was collected and washed with deionized water and ethanol for 3 times, respectively. Then the precursor was dried at 70 °C for 10 h in a vacuum oven. This typical precursor was labeled as sample A. The final product was obtained after a heat treatment in air at 700 °C for 4 h and the heating rate is 1 °C/min. The control experiments were carried out as listed in Table 1.

2.2. Characterization

X-ray powder diffraction (XRD) data for phase identification were collected at ambient temperature on a HUBER G670 (Cu $K_{\alpha1}$ radiation, $\lambda = 1.54056$ Å, Ge monochromator). The 2θ range was from 10° to 90° with the step of 0.005°. Morphology and particle size were observed by a scanning electronic microscope (SEM, JEOL JSM-6700F) operated with beam energy of 10 kV. Thermogravimetry–differential thermal analysis (TG–DTA) was carried out on a BOIF WCT-2D instrument under a continuous flow of air. The samples were analyzed at a heating rate of 5 °C/min to 800 °C. The excitation and emission spectra were obtained on a fluorescence spectrophotometer (Fluorolog-3, Jobin Yvon, France) with a xenon lamp as excitation source at room temperature at a step of 1 nm. And the decay curve was indentified on a Fluorescence Spectrometer (FLS920, Edinburgh).

3. Results and discussion

Fig. 1 shows XRD patterns of the precursor (sample A) and samples after calcinations. All the detectable diffraction peaks in Fig. 1a can be well indexed to hexagonal $Y(OH)_3$ (JCPDS card no. 83-2042). No second phase can be detected in the XRD pattern, which suggests that Eu^{3+} ions have been effectively built into the host lattice. All peaks shift towards the lower angle due to doping of larger Eu^{3+} ions (0.947 Å compared with 0.900 Å of Y^{3+} ions) [27], resulting in larger cell constants ($a = 6.269$ Å, $c = 3.549$ Å compared with $a = 6.261$ Å, $c = 3.544$ Å in JCPDS card no. 83-2042). Fig. 1b shows the XRD patterns of samples after calcinations at 500 °C, 600 °C, 800 °C and 1000 °C for 4 h, respectively. All diffraction peaks are in good agreement with cubic Y_2O_3 (JCPDS card no. 72-0927). As calcining temperature increases from 500 °C to 1000 °C, all diffraction peaks become stronger, indicating better crystallinity.

TG–DTA was carried out to investigate the physicochemical change of $Y(OH)_3$:Eu during heat treatment (Fig. 2). TG curve shows successive weight loss stages and the total weight loss is about 21.9%. The first weight loss (about 1.8%) is due to desorption of water molecules from the surface. The second weight loss with a sharp endothermic peak at 300 °C is attributed to the decomposition of $Y(OH)_3$ in Eq. (1). Next distinct weight loss with an endothermic peak at 410 °C is due to the conversion of YOOH to Y_2O_3 in Eq. (2) [28]. The experimental weight losses in the two reactions are 12.1% and 6.3%, which are very close to the theoretical values 12.8% and 7.3% calculated from two equations, respectively. The last weight loss (about 1.7%) may result from evaporation of residual water.

$$Y(OH)_3 \rightarrow YOOH + H_2O \quad (1)$$

$$2YOOH \rightarrow Y_2O_3 + H_2O \quad (2)$$

Morphology and particle size of the samples were investigated by SEM. Fig. 3a presents a panoramic SEM image of the flower-like $Y(OH)_3$:Eu microstructures (sample A). The microstructures are in the length of 5–7 μm and width of 2–3 μm. When observed from the top (Fig. 3b), the central part of the microstructure seems to be a hexagonal prism. When observed from the side, the top of the central prism is not flat but convex (Fig. 3c). There are six curving petals around the central prism and their surfaces are smooth. After calcinations, flower-like morphology is preserved and only involved in a slight decrease in size (Fig. 3d). The preservation of the morphology

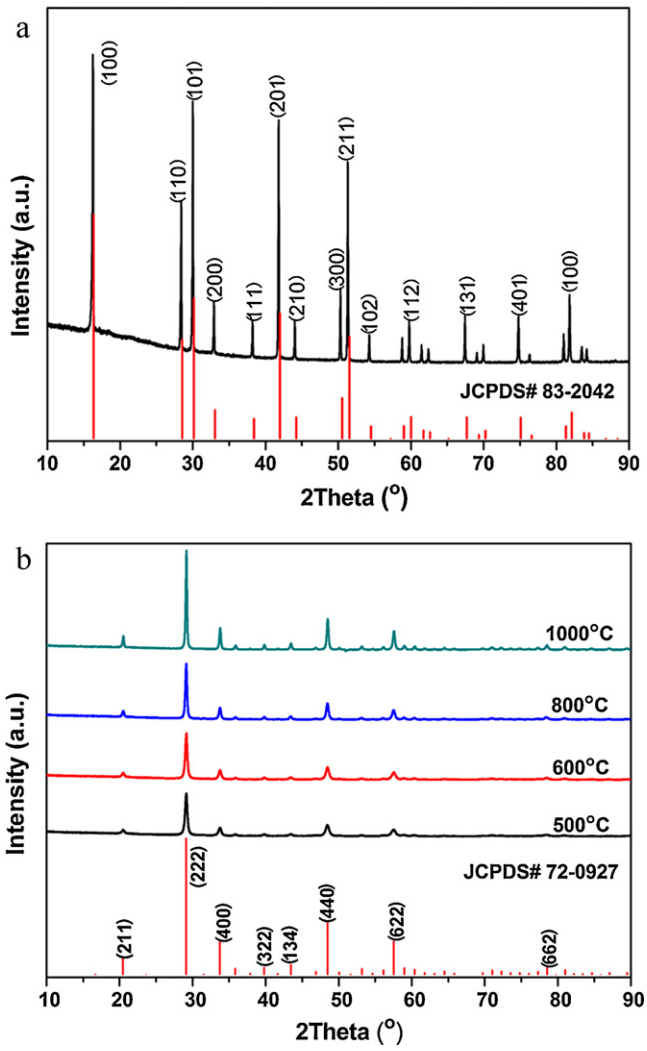

Fig. 1. XRD patterns of (a) sample A and (b) samples after calcinations at 500 °C, 600 °C, 800 °C, 1000 °C for 4 h.

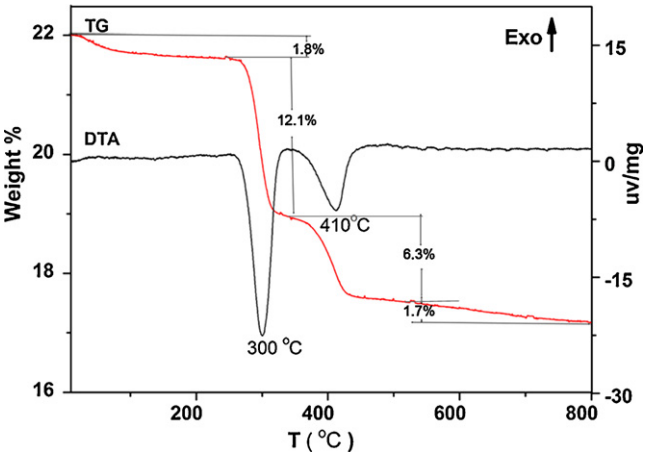

Fig. 2. TG–DTA curves of sample A.

Table 1
Experimental conditions for the preparation of different samples.

Sample	$Y(NO_3)_3$ (mmol)	$Eu(NO_3)_3$ (mmol)	$C_4H_4O_6KNa{\cdot}4H_2O$ (mmol)	NaOH (mol)	Hydrothermal temperature (°C)
A	1	0.05	1	0.02	210
B	1	0.05	0	0.02	210
C	1	0.05	0.5	0.02	210
D	1	0.05	1.5	0.02	210
E	1	0.05	1	0	210
F	1	0.05	1	0.01	210
G	1	0.05	1	0.03	210
H	1	0.05	1	0.04	210
I	1	0.05	1	0.08	210
J	1	0.05	1	0.02	150
K	1	0.05	1	0.02	190
L	1	0.05	1	0.02	230

is due to a slow heating rate of 1 °C/min. In this case, the atoms rearrangement and phase transition proceed gradually which would not cause the collapse of the flower-like microstructure.

To date, surfactant-assisted synthesis has attracted much attention in the field of morphology controllable synthesis [29–31]. In most cases, polymers surfactants and strong chelating ligands are used as structure-directing reagents. For example, sodium citrate [32] and ethylenediaminetetraacetic acid (EDTA) [33] are widely used as chelating reagents for the formation of novel microstructures, but the use of PSTT as a structure-directing reagent is not very common. To prove the importance of PSTT in our work, we investigated the influence of its concentration on the morphology of the precursor (Table 1, B–D). In the absence of PSTT, microrods with a length of 3–5 μm and diameter of about 100 nm are prepared (Fig. 4a, sample B). Similar result has been reported in our previous work [34] at 180 °C, but microrods prepared in this work are more uniform in size and also have smoother surface due to the higher hydrothermal temperature (210 °C). Once 0.5 mmol PSTT is added, microflowers with an average width of 5 μm are obtained (Fig. 4b, sample C). Interestingly, these microflowers are made of two layers (white arrows). When the amount of PSTT is increased to 1.5 mmol, morphology of product is similar to sample A (Fig. 4c, sample D). However, the microparticles are shorter compared with those in sample A, and their petals connect with each other. These results demonstrate that the PSTT concentration is an important factor for the formation of novel $Y(OH)_3$:Eu microstructures.

In addition, we believe the OH^- concentration can affect the nucleation and growth process of $Y(OH)_3$:Eu, which would further influence the morphology of hydrothermal product. In order to test our conjecture, the effect of NaOH concentration on the morphology of the precursor was also investigated (Table 1, E–I). Without NaOH (sample E), $Y(OH)_3$ nuclei are difficult to form due to lack of OH^- and the product is proved to be amorphous after phase analysis. When the amount of NaOH is 0.01 mol, microtubes with an average length of 15 μm and diameter of 3 μm are prepared (Fig. 5a, sample F), which is similar to previous report [35]. Increasing the amount of NaOH from 0.03 mol to 0.05 mol, the central part of flower-like microstructure becomes longer and larger, while six petals become shorter and smaller (Fig. 5b and c, sample G and H). Finally, six petals disappear completely (Fig. 5d, sample I) when the

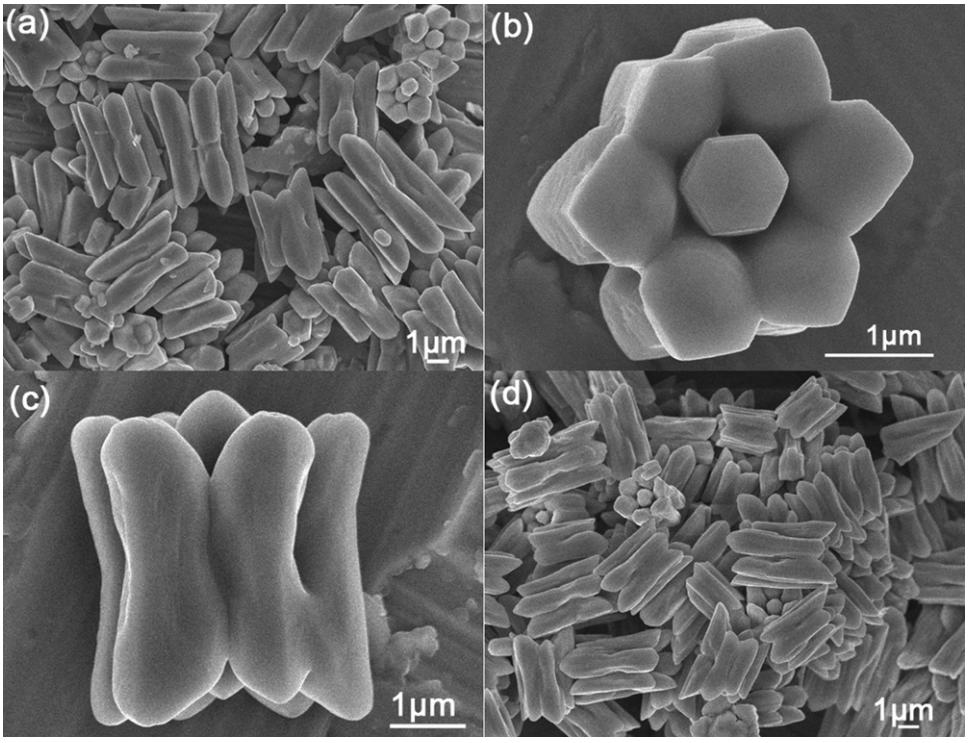

Fig. 3. SEM images of sample A: (a) a panoramic image; (b) magnified image from the top; (c) magnified image from the side; (d) after calcinations at 700 °C for 4 h.

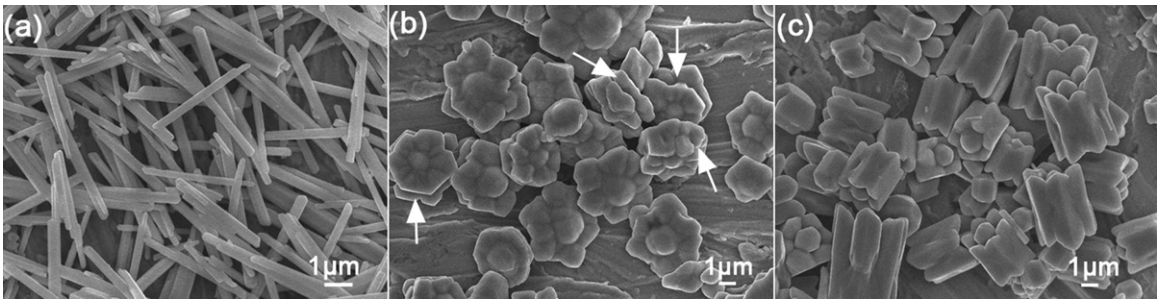

Fig. 4. SEM images of samples with different amount of PSTT: (a) B none; (b) C 0.5 mmol and (c) D 1.5 mmol.

amount of NaOH is increased to 0.08 mol, and most microstructures change into a football-like morphology. These results confirm our inference that NaOH concentration has marked effect on the growth process of $Y(OH)_3$:Eu microcrystals.

Moreover, temperature can affect the interaction between metal cations and chelating reagent, which may further influence the morphology of hydrothermal products. Therefore, experiments on temperature dependence were carried out (Table 1, sample J–L). When the temperature for hydrothermal synthesis is 150 °C, irregular aggregations is obtained (Fig. 6a, sample J). We believe that Y^{3+}/Eu^{3+} ions and PSTT form stable complex in the initial solution, so there is nearly no dissociative Y^{3+}/Eu^{3+} ions to form $Y(OH)_3$:Eu at this low temperature. When the temperature is increased to 190 °C, interactions between Y^{3+}/Eu^{3+} ions and PSTT are weakened and some Y^{3+}/Eu^{3+} ions are released. As a result, a little amount of product which has immature flower-like microstructures is obtained (Fig. 6b, sample K). Increasing the temperature to 230 °C, almost all the Y^{3+}/Eu^{3+} ions can be released, so a large amount of product is obtained. Compared with sample A (at 210 °C), the petals become longer but the basic morphology is the same (Fig. 6c, sample L). Based on the above results, we believe that metal cations and tartrate form stable complex in the initial solution and Y^{3+}/Eu^{3+} ions can be released to form $Y(OH)_3$:Eu above certain temperature.

To reveal the growth process of flower-like $Y(OH)_3$:Eu, time-dependent experiments were conducted. The products were collected at different reaction stages then their morphologies were investigated by SEM. When the hydrothermal reaction time is 2 h, amorphous white colloid is obtained (Fig. 7a). Prolonging reaction time to 3 h, most of the product is still colloid and only a little powder is obtained after centrifugation. Microparticles in this powder are polydispersed (Fig. 7b). We believe this is due to a low nucleate rate and a high growth rate. In this case, new nuclei continue to produce when early-formed nuclei have already grown into a large size [36]. In the sample obtained after 3 h, we find some microparticles with typical morphologies which can illustrate the crystal growth process at the initial stages (Fig. 7c–f). Firstly, irregular microparticles form (Fig. 7c), then they grow into larger ones which have round tops (Fig. 7d). Meanwhile, two layers of petals gradually grow from the side (Fig. 7e and f). In the sample obtained after 4 h, some immature flower-like microstructures which are similar to that in Fig. 6b can be observed (Fig. 7g and h). The round tops in Fig. 7e and f transform into a central prism, and each layer of the petals develops independently (Fig. 7g) until they link together

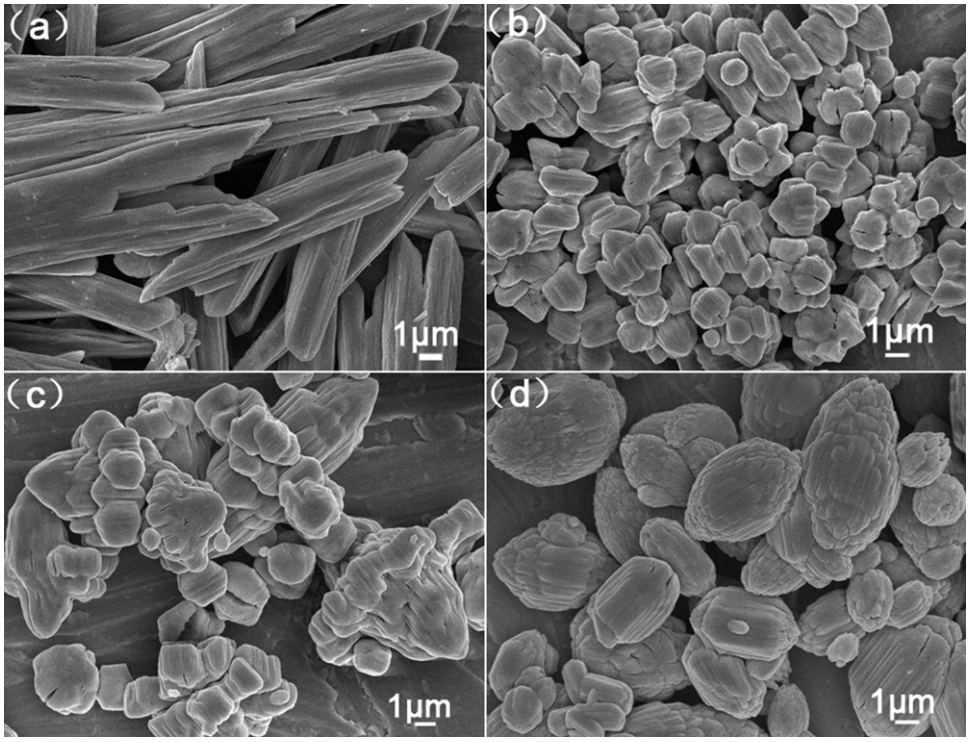

Fig. 5. SEM images of samples with different amount of NaOH after calcinations: (a) F 0.01 mol; (b) G 0.03 mol; (c) H 0.04 mol and (d) I 0.08 mol.

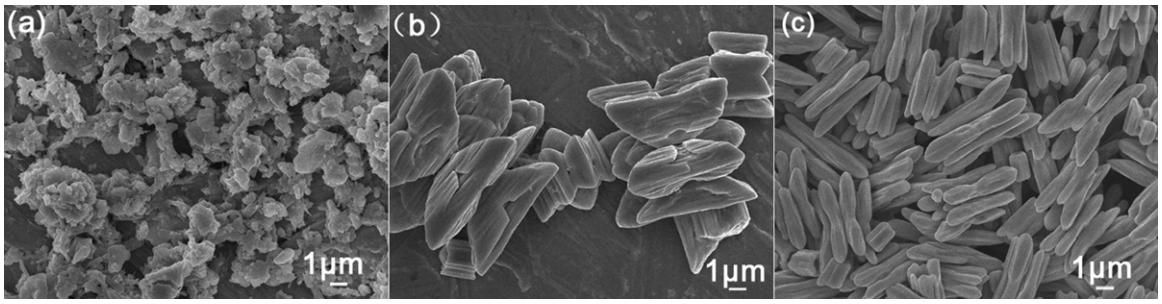

Fig. 6. SEM images of samples at different hydrothermal temperature after calcinations: (a) J 150 °C; (b) K 190 °C and (c) L 230 °C.

(Fig. 7h). There are some holes on the middle part of the petals, which demonstrate the middle part grow more slowly than the two ends. This phenomenon can successfully explain why the petals in Fig. 3c are curving. When the reaction is prolonged to 8 h, the size of microparticles is more uniform and the flower-like microstructures develop more completely (Fig. 7i). Increasing reaction time to 24 h and 36 h, the petals become larger and their surfaces are smoother (Fig. 7j–k). When reaction time is increased to 60 h, the big petals fall off from the central part, which leads to the collapse of flower-like microstructures (Fig. 7l).

As is well known, crystal growth is controlled by the intrinsic and extrinsic factors, including internal structure of a given crystal, and external conditions such as temperature, supersaturation, pH value of the solution and so on [37]. There are several

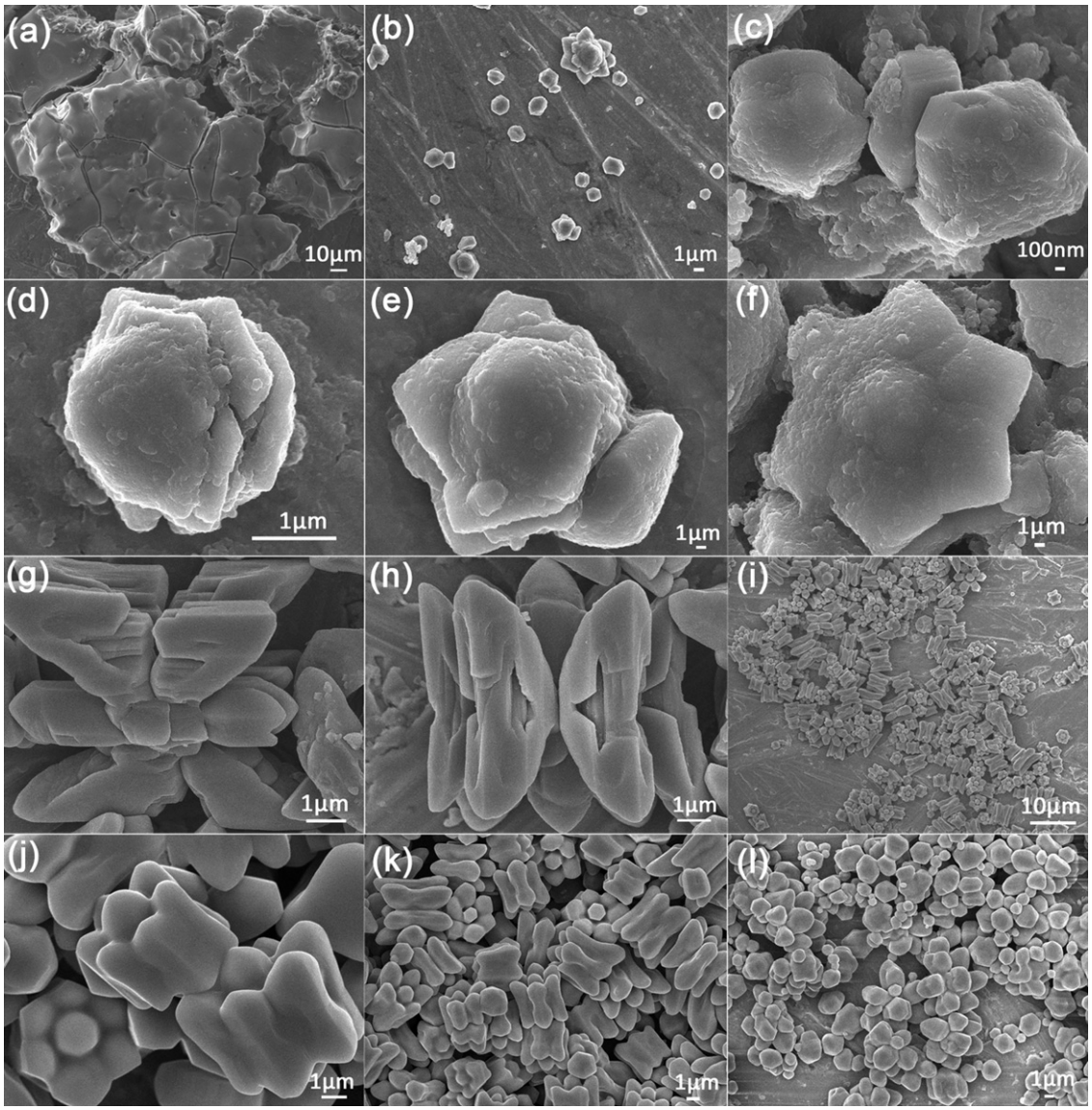

Fig. 7. SEM images of product obtained after different hydrothermal reaction time (a) 2 h; (b) 3 h; (c)–(f) microparticles found in (b); (g) and (h) microparticles found in product obtained after 4 h; (i) 8 h; (j) 24 h; (k) 36 h and (l) 60 h.

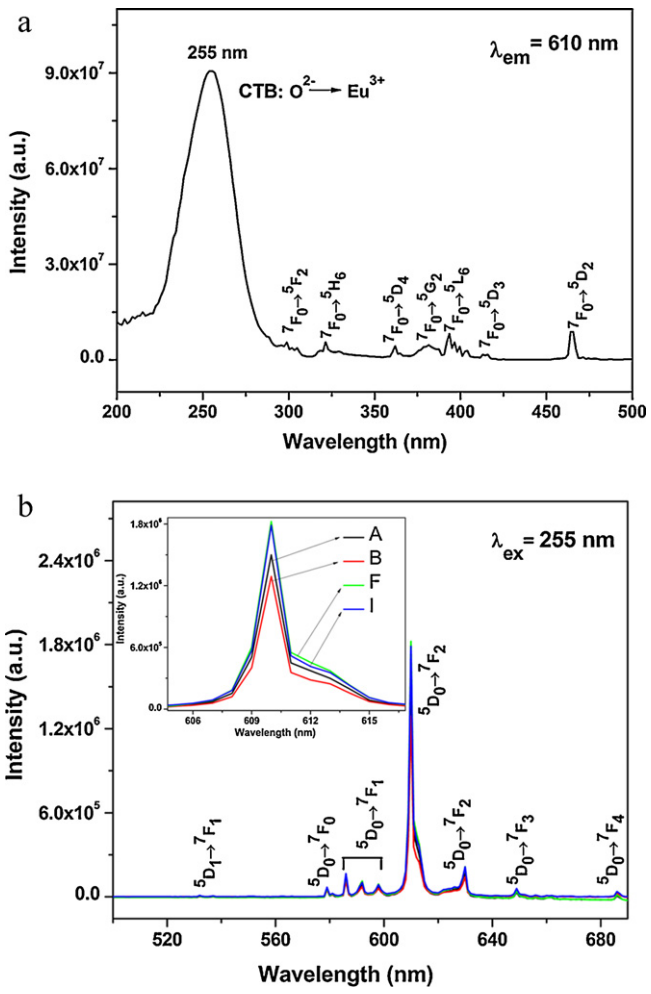

Fig. 8. (a) Excitation spectrum of sample A after calcinations at 700 °C and (b) emission spectra of Y_2O_3:Eu with different morphologies (sample A, B, F, I) after calcinations at 700 °C.

crystal growth mechanisms in the solution system [38], including the classical Ostwald ripening process [39], the oriented attachment mechanism [40], and the self-sacrificed template mechanism based on Kirkendall effect [41]. For the formation of flower-like $Y(OH)_3$:Eu microstructure, we believe the oriented attachment mechanism plays a key role. In this work, the round tops (Fig. 7d) which are formed at the initial stage tend to grow into central prisms. Meanwhile, $Y(OH)_3$:Eu growth units oriented attach to the side of the central prism to form six petals. Given a longer time, the petals become larger and their surfaces are smoother. Finally, the flower-like microstructures collapse.

Fig. 8a shows room-temperature photoluminescence (PL) excitation spectrum of flower-like Y_2O_3:Eu obtained from sample A after calcinations. The excitation spectrum (Fig. 8a) was recorded by monitoring emission at 610 nm. It consists of a broad band with a peak at 255 nm due to the charge transfer band (CTB) between O^{2-} and Eu^{3+} ions [19,42]. In the longer wavelength region, f–f transition peaks of Eu^{3+} ions (labeled in Fig. 8a) [16] can be detected with relatively weak intensity. Upon excitation at 255 nm, the emission spectra of Y_2O_3:Eu with different morphologies (sample A, B, F, I) were also recorded (Fig. 8b). The emission spectra contain a group of peaks, which are from $^5D_1$-$^7F_1$ and $^5D_0$-^7F_J ($J = 0, 1, 2, 3, 4$) transitions of Eu^{3+} ions, as labeled in Fig. 8b. Among them, the dominant red emission at 610 nm is attributed to the forced electric dipole transition ($^5D_0$-$^7F_2$) of Eu^{3+} ions while peaks at 586, 592, 598 nm are due to the allowed magnetic dipole transition ($^5D_0$-$^7F_1$) of Eu^{3+} ions. These emission peaks are in agreement with Zheng et al. [19] and Wang et al. [42] reports.

From the magnified graph of the dominate peak at 610 nm in Fig. 8b, we find the emission intensity of large microstructures (sample A, sample F and sample I) is higher than that of the microrods (sample B). This result is the same with our previous work [34]. We have noticed although the length of particles in sample B is in several micrometers, their diameter is still in nanoscale. Therefore, from our point of view, these particles may also be regarded as nanoparticles in some sense because their large surface to volume ratio. Some other literatures also report that microparticles have better luminescence performance than nanoparticles. In Paulraj et al. [43] research, they find the Y_2O_3:Eu microparticles have a higher PL efficiency than nanoparticles under the same measurement condition. They explain that the high scattering of light from nanomaterials is one important reason. They have observed that the diffused reflectance of nanocrystalline materials doubles that of microscale counterparts, which leads to a lower PL efficiency. In another report, Nelson et al. [44] have explored an alkalide reduction method for the preparation of Y_2O_3:Eu nanophosphor which has a PL efficiency far less than the microscale bulk material. The author explains that when the particle size is reduced, the surface becomes more accessible to the excitation centers, allowing for an increase in nonradiative surface recombination. This explanation is in accordance with Ronda's [45] opinion that the main drawback of nanoscale phosphors is their lower quantum efficiency compared with microsclae particles. This is attributed to the large surface area, which amplifies quenching processes. In addition, it is also believe that rodlike nanocrystal would possess more defects due to faster one-dimensional crystal growth [46], and these defects act as nonradiative centers which lead to its lower PL efficiency in our work.

However, we have realized the fact that reports on the PL efficiency of microphosphor compared with nanophosphor have always been ambiguous. Hirai et al. [47] have employed the reverse micellar systems and Ye et al. [48] have used a modified solution combustion method to synthesize nanocrystalline Y_2O_3:Eu material. These groups report that the PL emission of microphosphors has a higher PL efficiency than the nanoscale counterparts just like Paulraj et al. [43] and Nelson et al. [44] groups mentioned above. While Taxak et al. [49], Wakefield et al. [50] have adopted different methods for the preparation of nanocrystalline Y_2O_3:Eu and they report that PL efficiency of nanophosphor is better than the microscale bulk material. Therefore, there is no common idea towards this issue and the principles underlying still need further investigation.

Among the other three microstructures (Fig. 8b), the emission intensities of sample F (microtubes) and sample I (football-like microstructures) are almost equal and they are stronger than that of sample A (flower-like microstructures). It is probably because flower-like microstructures have several separated curving petals (Fig. 3a), which lead to an uneven surface and higher light scattering. Compared with flower-like microstructures, microtubes (Fig. 5a) and football-like microstructures (Fig. 5d) have relatively larger flat surface which will cause less scattering and lead to a stronger emission. This explanation is well supported by Paulraj et al. [43] conclusion that diffused reflectance can be a very important factor which affects the PL efficiency. These results also reveal that luminescent properties can be affected by the morphology of the phosphor particle. The influence of shape on the luminescent property of Y_2O_3:Eu can also be found in other literatures. For example, in Zhong et al. report [51], the emission intensities of microspheres, microtubes and microprisms are greatly different.

To investigate the effect of doping concentration on the emission intensity, Eu^{3+} ions doping concentration was changed. Fig. 9a shows the emission intensity of flower-like Y_2O_3:Eu with respect

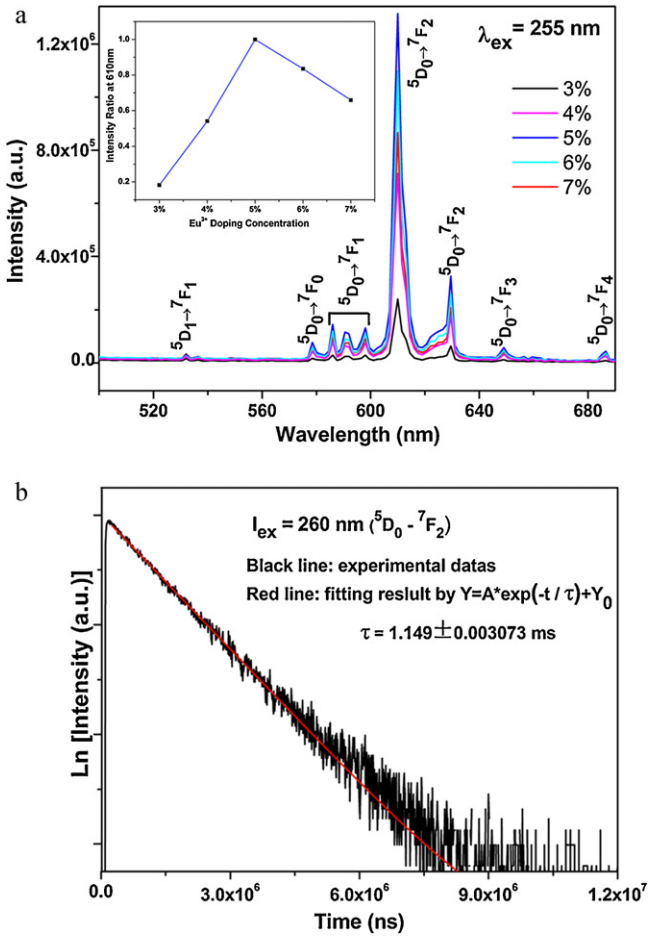

Fig. 9. (a) Emission spectra of Y_2O_3:Eu with different Eu^{3+} ions doping concentrations after calcinations at 700 °C, insert is relative intensity at 610 nm, set the emission intensity of 5 mol% Eu^{3+} ions doping as 1; (b) decay curve for the $^5D_0$-$^7F_2$ (610 nm) emission of Eu^{3+} in Y_2O_3: 5 mol% Eu flower-like microstructure after calcinations at 1000 °C.

to different doping concentration of Eu^{3+} ions. It is clearly to see that when the doping concentration is more than 5 mol%, emission intensity decreases due to quenching effect. The quenching effect might be attributed to cross-relaxation and resonance between the Eu^{3+} ions or due to paired Eu^{3+} ions. In our experiment, the highest emission intensity is obtained with 5 mol% Eu^{3+} ions doped. This result is consistent with the result given by Fu et al. [52], while in Hou et al. report [17], their optimum doping concentration is 9 mol%. This difference may result from the different synthesis methods.

The kinetic property for the luminescence of Y_2O_3: 5 mol% Eu flower-like microstructure after calcinations at 1000 °C was investigated by the decay curve (Fig. 9b). The decay curve for the luminescence of Eu^{3+} ions (monitored by $^5D_0$-$^7F_2$, 610 nm) can be well fitted into a single-exponential function. The lifetime of the Eu^{3+} ions is determined to be about 1.149 ms, which is basically in agreement with other Y_2O_3:Eu phosphors in previous reports [26,42].

4. Conclusions

In summary, flower-like $Y(OH)_3$:Eu microstructure has been successfully prepared through a facile hydrothermal process in the presence of potassium sodium tartrate as a structure-directing reagent. Y_2O_3:Eu with similar morphology can be obtained after sequential calcinations in air at 700 °C for 4 h. The concentration of reactants and the reaction temperature have a great influence on the formation of flower-like microstructure. An oriented attachment mechanism is proposed on the basis of time-dependent experiment. The prepared Y_2O_3:Eu sample exhibits a strong red emission at 610 nm and the emission intensity changes between samples with different shapes. The optimum concentrations for Eu^{3+} ions doping is determined to be 5 mol% and lifetime is about 1.149 ms. The present approach not only provides a pathway to fabricate novel microstructure of rare earth hydroxide and oxide but also helps to gain a deeper understanding about the crystal growth behaviors.

Acknowledgments

Financial supports from the National Natural Science Foundation of China (50990304), the National Basic Research Program of China (2007CB936704), the State '973' project (2009CB939903), the Major Basic Research Program of Shanghai (07DJ14001) and the Innovation Group for the Ministry of Science and Technology of China are gratefully acknowledged.

References

[1] J.F.A. Oliveira, T.M. Milao, V.D. Araujo, M.L. Moreira, E. Longo, M.I.B. Bernardi, J. Alloys Compd. 509 (2011) 6880–6883.
[2] H.Wang, G. Li, X. Guan, L. Li, J. Alloys Compd. 509 (2011) 4160–4166.
[3] J. Wang, Z. Zhang, J. Zhao, H. Chen, X. Yang, Y. Tao, Y. Huang, J. Mater. Chem. 20 (2010) 10894–10900.
[4] B. Zielinska, E. Borowiak-Palen, B. Grzmil, R.J. Kalenczuk, J. Alloys Compd. 509 (2011) 5414–5419.
[5] J.X. Liu, X.L. Dong, X.W. Liu, F. Shi, S. Yin, T. Sato, J. Alloys Compd. 509 (2011) 1482–1488.
[6] M. Tadic, N. Citakovic, M. Panjan, Z. Stojanovic, D. Markovic, V. Spasojevic, J. Alloys Compd. 509 (2011) 7639–7644.
[7] J. Gupta, K.C. Barick, D. Bahadur, J. Alloys Compd. 509 (2011) 6725–6730.
[8] S.B. Kulkarni, U.M. Patil, R.R. Salunkhe, S.S. Joshi, C.D. Lokhande, J. Alloys Compd. 509 (2011) 3486–3492.
[9] P. Ma, Y. Wu, Z. Fu, W. Wang, J. Alloys Compd. 509 (2011) 3576–3581.
[10] S.K. Sharma, A.I. Inamdar, Hyunsik Im., B.G. Kim, P.S. Patil, J. Alloys Compd. 509 (2011) 2127–2131.
[11] Q.L. Dai, M.E. Foley, C.J. Breshike, A. Lita, G.F. Strouse, J. Am. Chem. Soc. 133 (2011) 15475–15486.
[12] H.J. Liang, Y.D. Zheng, G.Y. Chen, L. Wu, Z.G. Zhang, W.W. Cao, J. Alloys Compd. 509 (2011) 409–413.
[13] X.P. Qin, G.H. Zhou, H. Yang, Y. Yang, J. Zhang, S.W. Wang, J. Alloys Compd. 493 (2010) 672–677.
[14] C.N. Wang, Y. Li, W.P. Zhang, M. Yin, Spectrochim. Acta, Part A 75 (2010) 8–13.
[15] J. Yang, Z.W. Quan, D.Y. Kong, X.M. Liu, J. Lin, Cryst. Growth Des. 7 (2007) 730–735.
[16] W.W. Zhang, M. Yin, X.D. He, Y.Q. Gao, J. Alloys Compd. 509 (2011) 3613–3616.
[17] X. Hou, S. Zhou, Y. Li, W. Li, J. Alloys Compd. 494 (2010) 382–385.
[18] Q. Pang, J.X. Shi, Y. Liu, D.S. Xing, M.L. Gong, N.S. Xu, Mater. Sci. Eng. B 103 (2003) 57–61.
[19] Y. Zheng, H. You, G. Jia, K. Liu, Y. Song, M. Yang, Y. Huang, H. Zhang, Cryst. Eng. Commun. 12 (2010) 585–590.
[20] G. Dong, Y. Chi, X. Xiao, X. Liu, B. Qian, Z. Ma, E. Wu, H. Zeng, D. Chen, J. Qiu, Opt. Express 25 (2009) 22514–22519.
[21] Y. He, Y. Tian, Z.F. Zhu, Chem. Lett. 32 (2003) 862–863.
[22] M. Yang, Y. Sui, S. Wang, X. Wang, Y. Wang, S. Lu, T. Lu, W. Liu, J. Alloys Compd. 509 (2011) 266–270.
[23] Z.G. Lu, D. Qian, Y.G. Tang, J. Cryst. Growth 276 (2005) 513–518.
[24] Y. Xiao, D.P. Wu, Y. Jiang, N. Liu, J.L. Liu, K. Jiang, J. Alloys Compd. 509 (2011) 5755–5760.
[25] S.L. Zhong, J.J. Chen, S.P. Wang, Q.Y. Liu, Y.L. Wang, S.J. Wang, J. Alloys Compd. 493 (2010) 322–325.
[26] M.K. Devaraju, S. Yin, T. Sato, Inorg. Chem. 50 (2011) 4698–4704.
[27] R.D. Shannon, Acta Cryst. A32 (1976) 751–767.
[28] R. Srinivasana, N.R. Yogamalara, J. Elanchezhiyanb, R.J. Joseyphusa, A.C. Bose, J. Alloys Compd. 496 (2010) 472–477.
[29] J.H. Zhang, H.Y. Liu, P. Zhan, Z.L. Wang, N.B. Ming, Adv. Funct. Mater. 17 (2007) 1558–1566.
[30] J.H. Warner, Adv. Mater. 20 (2008) 784–787.
[31] W.B. Bu, L.X. Zhang, Z.L. Hua, H.R. Chen, J.L. Shi, Cryst. Growth Des. 7 (2007) 2305–2309.
[32] X. Zhang, P. Hu, Y.B. Cao, W.C. Xiang, M.S. Yao, H.B. Zhang, F.L. Yuan, R.F. Xu, Cryst. Eng. Commun. 13 (2011) 3057–3063.
[33] J.H. Ha, P. Muralidharan, D.K. Kim, J. Alloys Compd. 475 (2009) 446–451.
[34] X.M. Zhang, M.L. Huang, Z.J. Zhang, B.Q. Liu, J.T. Zhao, Mater. Lett. 68 (2012) 269–272.

[35] Y.P. Fang, A.W. Xu, L.P. You, R.Q. Song, J.C. Yu, H.X. Zhang, Q. Li, H.Q. Liu, Adv. Funct. Mater. 13 (2003) 955–960.
[36] W. Feng, L.D. Sun, Y.W. Zhang, C.H. Yan, Coord. Chem. Rev. 254 (2010) 1038–1053.
[37] W.J. Li, E.W. Shi, W.Z. Zhong, Z.W. Yin, J. Cryst. Growth 203 (1999) 186–196.
[38] F. Lei, B. Yan, J. Phys. Chem. C 113 (2009) 1074–1082.
[39] L. Zhang, H. Wang, J. Phys. Chem. C 115 (2011) 18479–18485.
[40] Z.W. Wang, C. Schliehe, T. Wang, Y. Nagaoka, Y.C. Cao, W.A. Bassett, H.M. Wu, H.Y. Fan, H. Weller, J. Am. Chem. Soc. 133 (2011) 14484–14487.
[41] L.N. Ye, W. Guo, Y. Yang, Y.F. Du, Y. Xie, Chem. Mater. 19 (2007) 6331–6337.
[42] H. Wang, C.K. Lin, X.M. Liu, J. Lin, M. Yu, J. Appl. Phys. Lett. 87 (2005) 181907.
[43] A. Paulraj, P. Natarajan, K. Munnisamy, M.K. Nagoor, K.P. Nattar, B. Abdulrazak, J. Duraisamy, J. Am. Ceram. Soc. 94 (2010) 1627–1633.
[44] J.A. Nelson, E.L. Brant, M.J. Wagner, Chem. Mater. 15 (2003) 688–693.
[45] C.R. Ronda, Luminescence: From Theory to Applications, WILEY-VCH Verlag GmbH & Co. KGaA, Weinheim, 2008, p. 56.
[46] D. Chen, G.Z. Shen, K. Tang, Z.H. Liang, H.G. Zheng, J. Phys. Chem. B 108 (2004) 11280–11284.
[47] T. Hirai, Y. Asada, I. Komasawa, J. Colloid Interface Sci. 276 (2004) 339–345.
[48] X.Y. Ye, W.D. Zhuang, Y.S. Hu, T. He, X.W. Huang, J. Appl. Phys. 105 (2009) 064302.
[49] V.B. Taxak, S.P. Khatkar, S.D. Han, Rajeshkumar, Mukeshkumar, J. Alloys Compd. 469 (2009) 224–228.
[50] G. Wakefield, E. Holland, P.J. Dobson, J.L. Hutchison, Adv. Mater. 13 (2001) 1557–1560.
[51] S. Zhong, S. Wang, Q. Liu, Y. Wang, S. Wang, J. Chen, Mater. Res. Bull. 44 (2009) 2201–2205.
[52] Y.P. Fu, S.B. Wen, C.S. Hsu, J. Alloys Compd. 458 (2008) 318–322.